Protein Cage Nanoparticles Bearing the LyP-1 Peptide for Enhanced Imaging of Macrophage-Rich Vascular Lesions

Masaki Uchida,[†,§,∥] Hisanori Kosuge,[⊥,∥] Masahiro Terashima,[⊥] Deborah A. Willits,[‡,§] Lars O. Liepold,[†,§] Mark J. Young,[‡,§] Michael V. McConnell,[⊥] and Trevor Douglas[†,§,*]

[†]Department of Chemistry and Biochemistry, [‡]Department of Plant Sciences, and [§]Center for Bio-Inspired Nanomaterials (CBIN), Montana State University, Bozeman, Montana 59717, United States, and [⊥]Division of Cardiovascular Medicine, Stanford University School of Medicine, Stanford, California 94305, United States. [∥] These authors contributed equally to this paper.

ABSTRACT Cage-like protein nanoparticles are promising platforms for cell- and tissue-specific targeted delivery of imaging and therapeutic agents. Here, we have successfully modified the 12 nm small heat shock protein from *Methanococcus jannaschii* (*Mj*Hsp) to detect atherosclerotic plaque lesions in a mouse model system. As macrophages are centrally involved in the initiation and progression of atherosclerosis, targeted imaging of macrophages is valuable to assess the biologic status of the blood vessel wall. LyP-1, a nine residue peptide, has been shown to target tumor-associated macrophages. Thus, LyP-1 was genetically incorporated onto the exterior surface of *Mj*Hsp, while a fluorescent molecule (Cy5.5) was conjugated on the interior cavity. This bioengineered protein cage, LyP-Hsp, exhibited enhanced affinity to macrophage *in vitro*. Furthermore, *in vivo* injection of LyP-Hsp allowed visualization of macrophage-rich murine carotid lesions by *in situ* and *ex vivo* fluorescence imaging. These results demonstrate the potential of LyP-1-conjugated protein cages as nanoscale platforms for delivery of imaging agents for the diagnosis of atherosclerosis.

KEYWORDS: protein cage · nanoparticle · imaging agent · atherosclerosis · macrophage · cell-specific targeting

The development of imaging and therapeutic agents that target the cellular and/or molecular activity of a disease is highly desired since they will allow detection and treatment of the disease even at the earliest stages. Nanoscale supramolecular systems have been explored as delivery vehicles for imaging and therapeutic agents since nanoparticles have the potential to pass biological barriers that are generally more difficult for larger particles.[1−4] Among the supramolecular systems studied, protein cage architectures, such as viral capsids, ferritins, and small heat shock proteins, possess unique features not present in other systems such as micelles and liposomes.[5,6] As the protein cages are gene products, their size and structure are precisely controlled. Atomic resolution structural information of the cages allows us to design and modify desired sites on the proteins, either chemically or genetically, to impart directed functionality. This feature allows us to impart multifunctionality to a single platform by either utilization of amino acids with different chemical reactivity (*e.g.*, lysine and tyrosine) or combination of chemical and genetic modification techniques.[7−9] Since the protein shell acts as a barrier which discriminates between the interior cavity of the protein and the exterior environment, materials can be accumulated and sequestered within the protein cage. For instance, we can genetically introduce a cell-targeting peptide on the exterior of the cage and chemically load an imaging molecule on the inside of an identical protein cage.[7,9−17] In the present study, we have demonstrated the utility of a small heat shock protein cage isolated from *Methanococcus jannaschii* (*Mj*Hsp), which possesses a 12 nm exterior diameter and a 9 nm interior cavity,[18] as a platform for targeted delivery of an imaging agent to atherosclerosis, which could overcome current hurdles for the diagnosis of this disease.

Atherosclerosis is the underlying pathology of the majority of cardiac and vascular diseases, contributing to substantial morbidity and mortality in the U.S. and other developed countries.[19] Recent studies have revealed that atherosclerotic plaque destabilization, rather than plaque size, is the main cause of its rupture and following clinical consequences.[20,21] However, current clinical atherosclerosis imaging techniques can visualize vessel stenosis but offer limited information regarding the underlying biology within the vessel wall.

Accumulating evidence shows that inflammation, in general, and macrophages, in particular, play a pivotal role in the initiation, progression, and destabilization of atherosclerosis.[20−22] For this reason, macrophage

* Address correspondence to tdouglas@chemistry.montana.edu.

Received for review August 7, 2010 and accepted March 10, 2011.

Published online March 10, 2011
10.1021/nn102863y

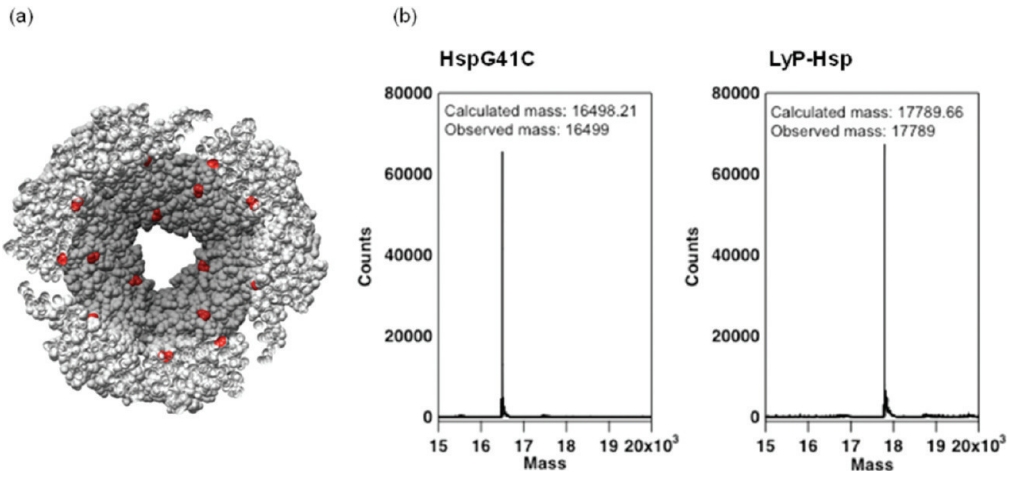

Figure 1. (a) Space filling representation of *Mj*Hsp half cut away view along with three-fold axis. Amino acid position 41, which is replaced with cysteine in the HspG41C and LyP-Hsp, is colored red. (b) ESI-Q-TOF mass spectrometry analysis of the HspG41C and LyP-Hsp. The calculated subunit mass of HspG41C and LyP-Hsp is 16 498.21 and 17 789.66, respectively.

cells in the vessel wall plaques are expected to be promising markers for detecting early stage atherosclerosis and assessing the risk of plaque rapture.[23] Using *in vivo* phage display, Ruoslahti and co-workers have identified an amino acid sequence, LyP-1 (CGNKRTRGC), that targets tumor-associated lymphatic vessels and macrophages.[24,25] We hypothesized that the LyP-1 peptide may also be able to target macrophage cells in the vessel wall. Thus, we have genetically introduced the LyP-1 peptide to the *Mj*Hsp to develop imaging agents with macrophage-targeting capability. Protein modeling, based on crystal structure of *Mj*Hsp, indicates the C-terminal of the protein is exposed on the exterior surface of the assembled cage.[18] Therefore, when the LyP-1 peptide is incorporated at the C-terminus of the *Mj*Hsp subunit, it is expected that the cage will present 24 copies of the targeting peptide on its exterior surface in a multivalent display.

In this paper, we have developed genetically engineered *Mj*Hsp cages with the LyP-1 peptide followed by incorporation of fluorescent molecules for imaging. The macrophage targeting of the engineered protein cages was evaluated *in vitro* and *in vivo*. For *in vivo* evaluation, fluorescence imaging of the localization of LyP-Hsp to macrophage-rich vascular lesions was examined using a mouse model.

RESULTS

Characterization of Hsp Protein Cages. The Hsp protein cage platform for this study was first engineered by replacing the glycine residue at position 41, located on the interior surface of the cage (Figure 1a), with cysteine (HspG41C)[26] to create a unique site-specific reaction site for attachment of imaging molecules. Then, the LyP-1 peptide was introduced at the C-terminus of the HspG41C (LyP-Hsp) as the targeting agent. Full amino acid sequences of HspG41C and LyP-Hsp are shown in Supporting Information Figure 1. Mass spectrometry (MS) analysis observed the subunit mass of HspG41C and LyP-Hsp to be 16 499 and 17 789, which matched well with the predicted mass of 16 498.21 and 17 789.66, respectively (Figure 1b). Transmission electron microscopy revealed that both the HspG41C and LyP-Hsp exhibited cage-like structures of about 13 nm diameter, and the two cages were morphologically indistinguishable (Figure 2). The elution volume on size exclusion chromatography of the LyP-Hsp was almost identical to that of HspG41C (data not shown). Dynamic light scattering (DLS) analysis demonstrated that the HspG41C and LyP-Hsp cages were both highly monodispersed in aqueous solution and there was no significant difference in hydrodynamic diameters between the two protein cages (Figure 2). Although the DLS data of the LyP-Hsp showed a minor population of a larger particle around 40−50 nm diameter, which could be due to aggregation of the protein cages, it was only 4% of the total particles. These protein cages were repurified after Cy5.5 conjugation, so that any aggregated material was removed. Together these results suggest that incorporation of the LyP-1 peptide into the C-terminus of the Hsp subunit does not interfere with self-assembly of the 24 subunits into a cage-like architecture, which is morphologically indistinguishable from the wild-type Hsp.

Conjugation of Fluorescent Dyes to Hsp Cages. As described above, the HspG41C and LyP-Hsp possess a unique cysteine residue at amino acid position 41, which is located on the interior surface of the cages (Figure 1a).[26] For *in vivo* fluorescence imaging, Cy5.5−maleimide dye was conjugated to the cysteine in the HspG41C and LyP-Hsp cages. HspG41C was reacted with various ratios of the Cy5.5−maleimide ranging from 0.3 to 3 molar equiv per subunit. The number of the dye molecules linked to the protein cages was

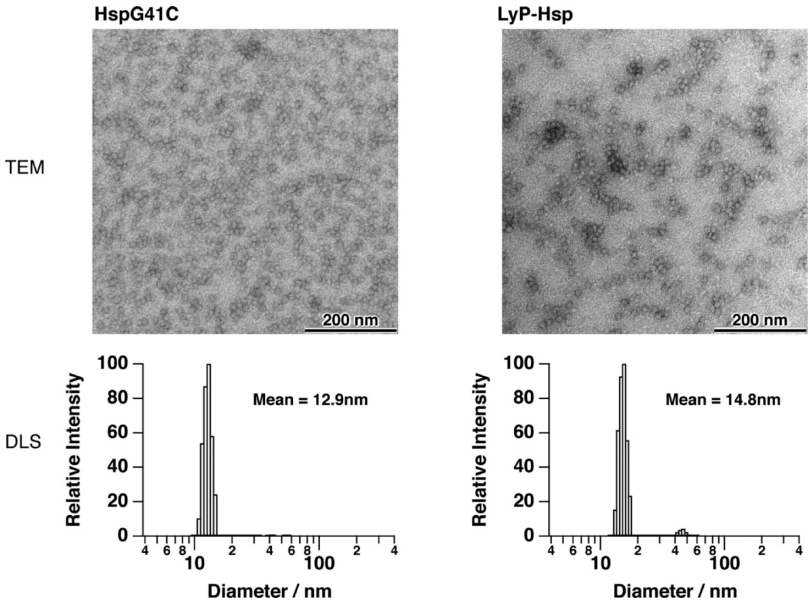

Figure 2. TEM images and DLS analysis of HspG41C and LyP-Hsp proteins after purification. Both proteins are indistinguishable from their morphologies.

determined from analysis of the absorbance spectra to be 0.12 dye/subunit (2.9 dye/cage), 0.24 dye/subunit (5.8 dye/cage), and 0.24 dye/subunit (5.8 dye/cage) when the input dye concentration was 0.3, 1, and 3 molar equiv per subunit, respectively. Fluorescence emission spectra of the Cy5.5-conjugated HspG41C measured under equivalent Cy5.5 concentrations revealed that the fluorescence intensity of the protein cages was significantly lower, compared to that of free Cy5.5, when the protein was reacted with higher concentration of Cy5.5 (1 or 3 dye/subunit) (Figure 3). This intensity decrease is probably due to self-quenching of the fluorescence signal due to crowding of the fluorescent molecules at the higher loadings. On the other hand, when the HspG41C was reacted with 0.3 dye/subunit, the protein cages still maintained about 75% fluorescence intensity of the same concentration of free Cy5.5. In the case of LyP-Hsp, when the protein cage was reacted with 0.3 Cy5.5/subunit, it was labeled with 0.13 dye/subunit (3.1 dye/cage) and its fluorescence emission intensity was comparable to that of the HspG41C reacted with same amount of Cy5.5 (Figure 3). Even though the LyP-Hsp has two additional cysteines in the LyP-1 peptide, the number of conjugated Cy5.5 is almost identical to HspG41C under the same reaction conditions. These data indicate that the two cysteines in the LyP-1 peptide do not participate in the conjugation reaction, suggesting the two cysteines are in the form of a disulfide bond and make the peptide a loop. This is further supported by MS analysis of iodoacetamide (IAA)-labeled cages, a reagent that is also specific for reaction with free thiols. Even though the HspG41C and LyP-Hsp were reacted with 10 mol excess IAA per protein subunit, most of the subunits of the LyP-Hsp as well as HspG41C were labeled with only

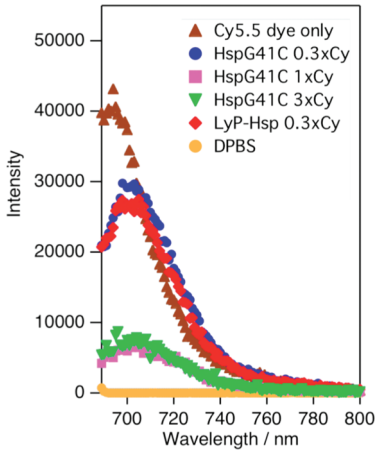

Figure 3. Fluorescence emission of the Hsp cages labeled with various concentration of Cy5.5−maleimide. The measurement was carried out under a constant Cy5.5 concentration (3 μM). The Cy5.5 quantities listed on the figure legend are input molar equivalents of the dye per subunit.

one IAA molecule and the subunits with two or more IAA were very minor (Supporting Information Figure 2). In addition, according to in-gel digestion and MS analysis, a spectral pattern around m/z = 596.6, which is well matched with the calculated isotope pattern of a peptide corresponding to amino acid 41 to 55 conjugated with one IAA ($C_{79}H_{126}N_{20}O_{23}S_2$), was clearly detected in the labeled LyP-Hsp and HspG41C samples (Supporting Information Figure 3). No fragments corresponding to IAA labeling of LyP-1 peptide were detected. These results clearly indicate that cysteine 41 residue, which is located inside of the LyP-Hsp cage (and HspG41C as well), is far more reactive than the two other cysteines included in the LyP-1 peptide part.

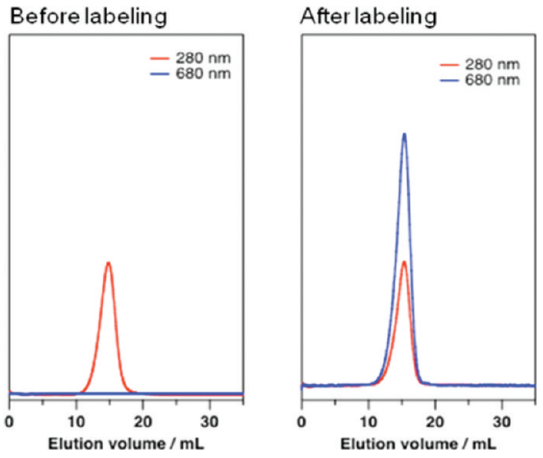

Figure 4. Size exclusion chromatography elution profile of HspG41C before and after labeling reaction with Cy5.5−maleimide. The postreaction profiles illustrate coelution of the HspG41C cage (280 nm) and Cy5.5 (680 nm).

The size exclusion chromatography profile of the Cy5.5-conjugated HspG41C was identical to that of the HspG41C without Cy5.5 except for the absorbance around 680 nm due to the Cy5.5 and indicates that the Cy5.5 labeling does not cause aggregation or disassembly of the Hsp protein cages (Figure 4).

When the HspG41C and LyP-Hsp were reacted with fluorescein−maleimide for the fluorescence-activated cell sorting (FACS) analysis, it was confirmed that they were labeled with 0.25 dye/subunit. The fluorescence emission intensities of the Hsp cages were comparable to that of free fluorescein under the same concentration (data not shown).

FACS Analysis of THP-1 Cells. When the THP-1 monocytes were not activated to differentiate into macrophages, neither HspG41C nor LyP-Hsp exhibited enhanced interaction with the cells. The geometric (geo.) mean fluorescence intensity value of cells incubated with HspG41C (3.2) or LyP-Hsp (4.6) was almost as low as the intrinsic autofluorescence of the cells (2.9) (Figure 5a). However, when the THP-1 cells were differentiated to macrophages by PMA activation,[27,28] the cells incubated with the LyP-Hsp showed much higher geo. mean fluorescence intensity (22.1) than the cell autofluorescence (3.1) (Figure 5b). On the other hand, the geo. mean value of the macrophages incubated with the HspG41C (4.2) was at the same level as the autofluorescence of the cells. This result clearly indicates that the LyP-Hsp exhibits enhanced affinity to macrophage cells but not to monocyte cells, while the HspG41C, which does not possess the macrophage-targeting peptide, exhibits no specific affinity to either monocyte or macrophage cells.

Fluorescence Imaging of Murine Vascular Lesions. This murine model produces macrophage-rich lesions in the ligated left common carotid arteries (LCCA), while the nonligated right common carotid arteries (RCCA) are unaffected (histology in Supporting Information Figure 4) (see Methods for more detailed procedure).[29] The fluorescence signal from the Cy5.5-conjugated Hsp cages was evaluated by *in situ* and *ex vivo* imaging of the neck region 48 h after intravenous injection. Both *in situ* and *ex vivo* imaging demonstrated much higher signal in the LCCA than the RCAA, clearly indicating selective accumulation of the LyP-Hsp in the macrophage-rich LCCA rather than in the control RCAA (Figure 6a). In contrast, HspG41C-injected mice showed a more modest increase in fluorescence signal in the LCCA. The Maestro imaging system is sensitive to displaying the brightest part of the image. Thus, the LyP-Hsp image shows the bright area in the LCCA and limited signal elsewhere. The HspG41C image does not have a strong focal enhancement, so the image shows more uniform signal throughout the LCCA, RCCA, and aortic arch. For both the *in situ* and *ex vivo* images, the quantitative analysis uses the L *versus* R ratio to account for any background signal differences. Quantitative comparison of *ex vivo* fluorescence signal from LCCA and RCCA revealed that the LCCA/RCCA signal ratio of the LyP-Hsp-injected mice was nearly eight times higher than that of the HspG41-injected mice ($p = 0.0002$) (Figure 6b). Confocal microscope images of immunofluorescently stained LCCA illustrate that LyP-Hsp labeled with Cy5.5 (red signal) colocalized with macrophages (green signal) in merged images (Figure 7). These results suggest that the LyP-Hsp has significant targeting capability toward macrophage-rich vascular lesions as compared to the HspG41C in our experimental mouse model.

DISCUSSION

We have demonstrated that a cage-like protein nanoparticle genetically engineered with LyP-1 significantly enhances imaging of vascular macrophages in a mouse model system. This is the first demonstration that LyP-1 targets vascular macrophages and can be used with protein cages to enhance imaging of vascular inflammation. Since macrophages are believed to be key players in inflammation of atherosclerosis,[20−22] imaging of macrophages could be a promising strategy to detect plaques and/or evaluate high-risk lesions.[23,30,31] Other macrophage-targeting moieties have been investigated, such as scavenger receptor,[32] chemokine receptor CCR-2[33] and matrix metalloproteinase.[34] In the present study, we have examined the multivalent display of the LyP-1 peptide coupled with fluorescently labeled *Mj*Hsp cages. The LyP-1 peptide has previously been identified to target tumor-associated macrophage cells.[24,25] Here we show, by fluorescence imaging studies, that this peptide can also target macrophages in experimental atherosclerosis lesions in a mouse model system. We have previously shown that a protein cage conjugated with RGD-4C peptide,[35] which binds selectively to integrin $\alpha_v\beta_3$, has

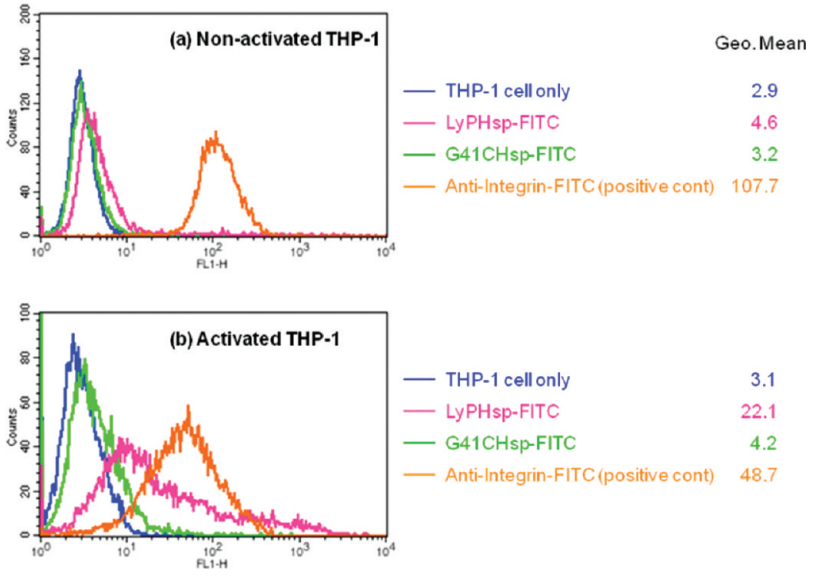

Figure 5. FACS analysis of THP-1 cells as nonstimulated monocytes (a) or PMA-stimulated macrophages (b) after incubation with fluorescence-labeled Hsp protein cages. The data are plotted as histograms with their corresponding geometric (geo.) mean fluorescence values. The LyP-Hsp exhibited enhanced interaction with THP-1 macrophages compared to monocytes, whereas HspG41C did not show specific interaction with either cell type.

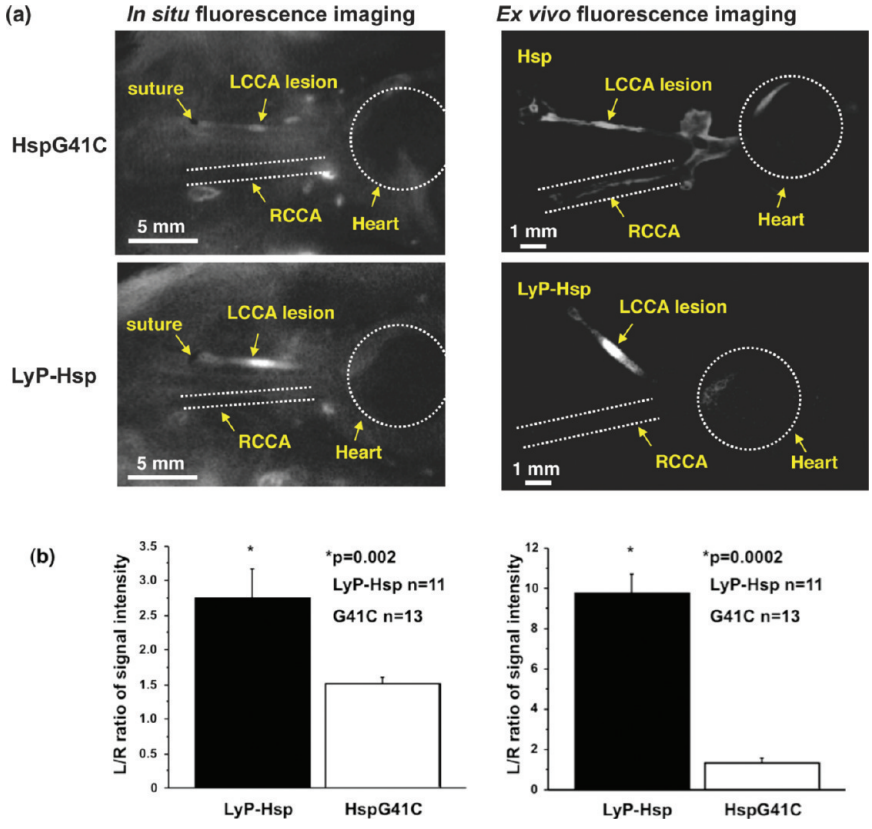

Figure 6. (a) *In situ* and *ex vivo* fluorescence imaging of the mice after 48 h of Cy5.5-labeled HspG41C or LyP-Hsp injection. In both the *in situ* and *ex vivo* images, the LyP-Hsp-injected mouse provided more intense fluorescence signal from the left common carotid artery (LCCA) than the right common carotid artery (RCAA). (b) Fluorescence signal intensity ratio of LCAA/RCAA obtained from *in situ* and *ex vivo* images. The LyP-Hsp-injected mice showed higher LCAA/RCAA than the HspG41C-injected mice.

specific affinity to THP-1 cells *in vitro*.[36] It should be noted that there is an interesting difference between the LyP-1 peptide and the RGD-4C peptide in their cell-targeting behavior. The LyP-1-conjugated protein exhibits specific affinity to the THP-1 cells only when the cells are activated and differentiated to macrophage,

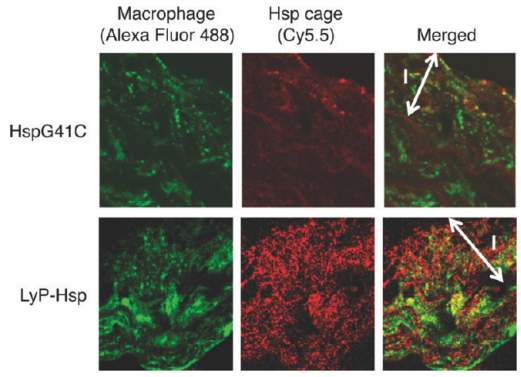

Figure 7. Confocal images of left carotid arteries. Cy5.5-conjugated LyP-Hsp (red) were colocalized (yellow) with macrophages labeled with Alexa Fluor 488 (green) compared to Cy5.5-conjugated HspG41C. I: neointima.

while the RGD-4C-conjugated protein shows affinity to even nonactivated THP-1 cells. These data clearly indicate that cellular receptors for the two peptides are different. Indeed, p32 (alternatively known as gC1q) has recently been identified as the cellular receptor for the LyP-1 peptide.[25] Although, to the best of our knowledge, the relationship between vascular macrophage cells and p32 protein has not yet been revealed, it will be important to compare *in vivo* targeting efficiency and cellular uptake pathways between the LyP-1-conjugated protein cages and the RGD-4C-conjugated protein cages. A dissociation constant K_d of the LyP-1 and p32 interaction was determined as 3 μmol/L.[25] The LyP-Hsp displays 24 copies of the LyP-1 peptide on its surface, and this multivalent display would be beneficial to enhance the modest affinity of the LyP-1 peptide to p32, similar to what was observed on interaction between multivalent RGD peptides displayed on nanoparticles and integrin-up-regulated cells.[37]

Although we successfully incorporated Cy5.5 dye inside of the Hsp cages *via* the engineered interior cysteine residue, the maximum number of dye molecules that could be conjugated was determined to be 0.24/subunit (5.8/cage). One possible reason why the maximum number of the dye incorporated inside of the cage was not 1 but 0.24/subunit is bulkiness of the Cy5.5−maleimide dye. It is assumed that access of the dye to the interior of the cage is *via* eight pores (~3 nm diameter) of the cage around the three-fold axes of the protein cage. As shown in the Figure 1a, the cysteine position 41, where the dye is conjugated, is located around the pores. Since the Cy5.5−maleimide dye is fairly bulky (MW = 1153.5), if one dye is linked to a cysteine around the pore, it would make the pore less accessible for other dye molecules. However, we believe the more significant limitation of the material we have used in the current experiment is self-quenching of the fluorescence signal due to crowding of the dye inside of the cage. Therefore, utilization of a protein cage with a larger interior cavity might be one potential approach to improve fluorescence intensity per protein cage.

Another critical limitation is inherent in fluorescence imaging. While fluorescence imaging was able to demonstrate targeted macrophage imaging with LyP-Hsp in an *in vivo* mouse model, it is not a standard clinical imaging modality due to limited tissue penetration. Noninvasive small animal imaging may be improved through more sensitive fluorescence imaging techniques, such as fluorescence molecular tomography.[38] More importantly, exploitation of the protein cages as platforms for imaging agents is not limited to fluorescence imaging. A variety of imaging techniques such as MRI,[29,39−43] CT,[44] PET,[31] SPECT,[31] and combinations of thereof[45−48] have been studied to detect macrophages in atherosclerosis. Protein cages could be ideal containers to load imaging agents for these techniques, as well.[12,14,49−53] Furthermore, therapeutic drugs for atherosclerosis could be incorporated into the cage constructs for targeted delivery,[54,55] so that the protein cages can be "theranostic" platforms.

Investigation of biocompatibility and biodistribution of the protein cages *in vivo* is critical for future clinical translation.[13,56−58] We have recently reported that, in both naïve and immunized mice, *Mj*Hsp shows broad distribution throughout most tissue and organs, followed by rapid clearance and the absence of long-term persistence within the tissue and organs.[58] It is interesting to note that, despite the reported rapid clearance of the protein, significant fluorescence signal from the Cy5.5-labeled LyP-Hsp was observed on the ligated LCAA after 48 h of injection. It is assumed that accumulation of the LyP-Hsp in the vascular lesions is due to the LyP-1 peptide, maintaining a high fluorescence signal, whereas the cages with no targeting are cleared from tissues within 48 h. As a result, signal intensity contrast from the LCAA *versus* other tissues may be enhanced even further after 48 h of injection. More detailed biocompatibility assessment of *Mj*Hsp, such as blood half-life and immunogenicity, and comparison with other protein cages, such as human ferritin or viral capsids, require further investigation.

CONCLUSION

A cage-like protein-based nanoparticle that possesses a macrophage-targeting peptide, LyP-1, and a fluorescence imaging molecule has been developed without disrupting the overall structure of a platform protein, *Mj*Hsp. *In vitro*, fluorescently labeled LyP-Hsp exhibits specific interaction with macrophages and not monocytes, while the HspG41C (without LyP-1) does not. *In vivo*, macrophage-rich carotid lesions in mice showed high *in situ* and *ex vivo* fluorescence signal

after LyP-Hsp injection compared to the HspG41C injection. These findings hold the promise that LyP-1-conjugated protein cages could be useful for *in vivo* delivery of imaging agents for detection and characterization of atherosclerosis guided by biological activity in the vessel wall.

METHODS

Cloning of *Mj*Hsp 16.5 and Genetic Engineering of HspG41C. *Methanococcus jannaschii* genomic DNA was obtained from the American Type Culture Collection (ATCC; 43067). As described previously,[26] the gene encoding the small heat shock protein (*Mj*Hsp16.5) was amplified by polymerase chain reaction (PCR) and cloned into the pET-30a(+) vector (Novagen, Madison, WI). Two rounds of site-directed mutagenesis were performed with the *Mj*Hsp16.5 plasmid in order to (1) make it possible to insert additional amino acid sequence at the C-terminus and (2) to introduce a unique reaction site. The stop codon directly upstream of the *Bam*HI site was deleted by PCR-mediated site-directed mutagenesis in order to make it possible to easily insert additional amino acid sequence at the C-terminus. In order to introduce a unique reaction site into the *Mj*Hsp16.5, the glycine at position 41 was changed to cysteine (HspG41C).[26] The resulting plasmid vector was transformed into XL2 Blue ultracompetent *Escherichia coli* (Stratagene, La Jolla, CA) and plated on LB with kanamycin plates for selection. Positive colonies were grown overnight in 3 mL of LB with 30 mg/L kanamycin medium. Plasmid DNA was isolated using Perfectprep Plasmid Mini (Effendorf, Hamburg, Germany), and inserted DNA was sequenced on an ABI 310 automated capillary sequencer using Big Dye chain termination sequence technology (Applied Biosystem, Foster City, CA).

Mutagenesis of LyP Peptide-Conjugated HspG41C (LyP-Hsp). The plasmid described above was used to incorporate the LyP-1 peptide sequence onto the C-terminus of the HspG41C by insertion into the *Bam*HI site on the plasmid. The complementary primers with overhanging gatc, 5′ ga tct gga gga tgt ggc aac aaa cgc a**cc cgg g**gc tgc gga taa gga 3′ and 5′ g atc tcc tta tcc gca gc**c ccg gg**t gcg ttt gtt gcc aca tcc tcc a 3′, were designed. Boldfacing delineates a *Sma*I site used for screening. The primers were mixed at a 1:1 molar ratio, annealed, and treated with kinase. The primer set was subsequently ligated with an alkaline phosphatase-treated, *Bam*HI-digested HspG41C plasmid overnight at 17 °C. The LyP-Hsp plasmid was isolated and sequenced as described above for the HspG41C. This insertion of the LyP-1 peptide sequence resulted in the change of the original C-terminus amino acid sequence of HspG41C from *GINIE-stop* to *GINIEGSGGCGNKRTRGCG-stop*.

Expression and Purification of Hsp. The HspG41C and LyP-Hsp proteins were obtained using a heterogeneous expression system in *E. coli*. One liter cultures of *E. coli* (BL21 (DE3), Novagen) transformed pET-30a(+) of HspG41C or LyP-Hsp plasmid were grown overnight in LB medium with 30 mg/L kanamycin. For the LyP-Hsp expression, the protein production was induced by IPTG to a final concentration of 1 mM when o.d. 600 nm of the culture medium reached 0.8. Cells were cultured overnight after the induction. After the incubation, cells were collected by centrifugation, and then the pellets were resuspended in 20 mL of a lysis buffer (50 mM HEPES, 100 mM NaCl, pH 7.5). Lysozyme, DNase, and RNase were added to final concentrations of 50, 60, and 100 μg/mL, respectively. After 1 h incubation at room temperature, the cell suspension was treaded with French press followed by sonication on ice. The *E. coli* debris was removed *via* centrifugation. The supernatant was heated at 60 °C for 10 min, thereby precipitating many of the *E. coli* proteins, which were removed by centrifugation. The supernatant was dialyzed into a buffer of 100 mM HEPES, 1 M NaCl, pH 7.5 overnight followed by centrifugation. The supernatant was subjected to size exclusion chromatography (SEC; Amersham-Pharmacia, Piscataway, NJ) with a Superose 6 column to purify HspG41C and LyP-Hsp.

Characterization of Hsp. The purified Hsp samples were analyzed by ESI-Q-TOF mass spectrometry (MS; Q-TOF Premier, Waters) interfaced to a Waters UPLS and autosampler. The samples were injected onto a BioBasic SEC-300 column and eluted with a buffer of 59.9% water, 40% isopropyl alcohol, and 0.1% formic acid isocratically with a flow rate of 25 μL/min. Mass spectra were acquired in the range of m/z = 50−5000 and processed using component analysis from MassLynx version 4.1 from multiple charge state distributions. Protein concentration was determined by absorbance at 280 nm divided by the reported extinction coefficient (9322 M^{-1} cm^{-1} for subunit, 223 728 M^{-1} cm^{-1} for entire cage). The Hsp protein cages were also routinely characterized by SEC, SDS-PAGE, dynamic light scattering (DLS; Brookhaven, 90Plus particle size analyzer), and transmission electron microscopy (TEM; LEO 912AB).

Conjugation of Hsp Cages with Fluorescence Molecules. The HspG41C and LyP-Hsp were both conjugated with two different fluorescence dyes independently, either Cy5.5−maleimide dye (GE Healthcare UK limited, Amersham, UK) for *in vivo* fluorescence imaging or fluorescein-5−maleimide dye (Molecular Probes, Eugene, OR) for *in vitro* fluorescence-activated cell sorting (FACS). The engineered internal cysteine at the position 41 was utilized for the conjugation. For the Cy5.5 labeling, the protein (1 mg/mL in Dulbecco's phosphate buffered saline (DPBS) at pH 7.0) was reacted with the dye in a concentration of 0.3−3 molar equiv per subunit at room temperature for 2 h followed by overnight incubation at 4 °C. The proteins were purified by SEC with DPBS at pH 7.4 to remove unreacted free dye. For the fluorescein labeling, the proteins (1 mg/mL in DPBS at pH 7.0) were reacted with the dye in a concentration of 6 molar equiv per subunit at room temperature for 2 h followed by overnight incubation at 4 °C. Fluorescence emission spectra of the Cy5.5-labeled protein cages in DPBS at pH 7.4 were measured with a fluorimeter (TECAN Safire, Männedorf, Switzerland). Excitation wavelength, excitation, and emission bandwidth were set at 678, 2.5, and 5.0 nm, respectively. Emission wavelength was scanned from 689 nm.

Iodoacetamide (IAA) Labeling of Hsp Cages and Their In-Gel Digestion Analysis. The HspG41C has only one cysteine at amino acid position 41, whereas the LyP-Hsp has two additional cysteines in the engineered LyP-1 peptide part. Although we assume these two cysteines form internal disulfide linkage, we investigated the reactivity of the cysteines by labeling them with IAA. The HspG41C and LyP-Hsp (3 mg/mL in 50 mM sodium phosphate, 100 mM NaCl, 5 mM EDTA at pH 7.85) were reacted with 50 mM IAA dissolved in the same buffer in a concentration of 10 molar equiv per subunit at room temperature for 3 h. The proteins were purified by Micro Bio-Spin column (Bio-Rad, Hercules, CA) with DPBS at pH 7.4 to remove unreacted IAA. The samples were electrophoresed in a SDS gel, and bands corresponding to the expected mass of the HspG41C and LyP-Hsp subunits were subjected to in-gel digestion according to previous literature.[59] The extracted peptides were analyzed by ESI-Q-TOF Premier mass spectrometer (Waters). The samples were injected onto a C18 column (NanoEase, 100 μm × 100 mm, BEH130, Waters) and eluted with a water/acetonitrile linear gradient (eluent A: 0.1% formic acid in water, eluent B: 0.1% formic acid in acetonitrile) with a flow rate of 0.9 μL/min. Protein Lynx Global Server (PLGS 2.1, Waters) was used to process the LC/MS^E data and return protein identifications and peptide modification data.

***In Vitro* Evaluation of Macrophage-Targeting Capability of LyP-Hsp.** The macrophage-targeting capability of genetically engineered LyP-Hsp was studied with FACS *in vitro*. Human monocyte cell line, THP-1,[60] was purchased from ATCC. The cells were cultured in PRMI 1640 supplemented with 10% fetal bovine serum,

100 U/mL of penicillin, 100 μg/mL of streptomycin, and 0.05 mM of 2-mercaptoethanol at 37 °C in 5% CO_2 atmosphere. In order to differentiate the monocyte cells into macrophages, a subset of the THP-1 cells was activated in the presence of 100 nM phorbol 12-myristate 13-acetate (PMA) 2 days in advance of the FACS analysis.[27,28] As the activated THP-1 cells adhered on cell culture dishes, the cells were washed with PBS (without Ca^{2+} and Mg^{2+}) and then detached from the dishes using Accutase (Sigma) at 37 °C for 15 min before further experiments.[28] Both nonactivated and activated THP-1 cells were harvested by centrifuge at 1000 rpm for 5 min. For the FACS analysis, either nonactivated or activated cells suspended in DPBS (with Ca^{2+} and Mg^{2+}) at a concentration of 2.5×10^6 cell/mL were incubated with fluorescein-conjugated Hsp cages on ice for 20 min under normalized fluorescein concentration (2 μM). After the incubation, the cells were washed two times with DPBS (with Ca^{2+} and Mg^{2+}) and then resuspended in DPBS (with Ca^{2+} and Mg^{2+}). The fluorescein-conjugated anti-integrin $\alpha_v\beta_3$ mAb (Chemicon MAB1976F) was used as a positive control since the THP-1 cells express integrin α_v.[61] Flow cytometry was performed on a FACSCalinur, (BD Biosciences, Mountain View, CA) and analyzed using Cell Quest software. Each cell sample was sorted until 10 000 event counts.

Preparation of Mouse Model of Vascular Inflammation. Macrophage-rich vascular lesions were induced in 24 FVB strain mice (Supporting Information Figures 4 and 5). Mice were fed a high-fat diet containing 40% kcal fat, 1.25% (by weight) cholesterol, and 0.5% (by weight) sodium cholate (D12109, Research Diets, Inc. New Brunswick, NJ).[29,62] After 4 weeks of high-fat diet, mice were rendered diabetic by administration of 5 daily intraperitoneal injections of streprozotocin (STZ), 40 mg/kg in citrate buffer (0.05 mol/L, PH4.5, Sigma-Aldrich). After 5 injections of STZ, serum glucose level of each mouse was measured from tail vein blood using a glucometer. If the glucose level was below 200 mg/dL, the mice were injected with additional STZ for 3 consecutive days. Two weeks after the first STZ injection, the left common carotid arteries (LCCA) were ligated ($n = 24$) below the bifurcation with the use of 5−0 silk ligature (Ethicon) under 2% inhaled isoflurane. The wound was closed by suture, and the animals were allowed to recover on a warming blanket. The right common carotid arteries (RCCA) were not ligated and served as internal controls. All procedures were approved by the Administrative Panel on Laboratory Animal Care at Stanford University.

***In Vivo* Evaluation of LyP-Hsp-Targeting Capability to Vascular Macrophages.** Two weeks after carotid ligation, the mice received intravenous injection of Cy5.5-labeled HspG41C (n = 13) or LyP-Hsp (n = 11) (8 nmol of Cy5.5/mouse) *via* tail vein. Under inhalational anesthesia (2% isoflurane), all mice underwent imaging 48 h after injection using the Maestro *in vivo* imaging system (CRi, Woburn, MA), which has the capability to separate fluorochromes from autofluorescence based on multispectral analysis. Both *in situ* and *ex vivo* fluorescence imaging of the carotid arteries were performed. For *in situ* fluorescence imaging, animals were euthanized and left and right carotid arteries were surgically exposed. After *in situ* fluorescence imaging, carotid arteries were carefully removed en bloc for *ex vivo* fluorescence imaging. In order to compare the targeting capability of the HspG41C and LyP-Hsp for diseased (ligated) LCCA *versus* control (nonligated) RCCA, the ratio of LCCA to RCCA fluorescence signal intensity from the same mice was calculated. Statistics were calculated using Student's t test.

Histology of Carotid Arteries. Immediately after fluorescence imaging, carotid arteries were embedded in optimum cutting temperature (OCT) compound (Sakura Finetek USA, Inc., Torrance, CA) and flash frozen in liquid nitrogen. Frozen sections (5 μm) were fixed in acetone for 10 min at 4 °C. After a washing in PBS, they were incubated with antimouse Mac-3 antibody (BD Biosciences, San Jose, CA) overnight at 4 °C. Sections were then incubated with biotinylated secondary antibodies at room temperature for 30 min. Antigen−antibody conjugates were detected with avidinbiotin−horseradish peroxidase complex (Vector Laboratories, Burlingame, CA) according to the manufacturer's instructions. 3-Amino-9-ethylcarbazole was used as chromogen, and sections were counterstained with hematoxylin.

Immunofluorescence double staining was performed to confirm colocalization of macrophages and Cy5.5-conjugated Hsp cages. After incubation with antimouse Mac-3 antibody overnight at 4 °C, sections were stained with Alexa Fluor 488-conjugated anti-rat IgG (Molecular Probes, Eugene, OR) at room temperature for 2 h. Sections were observed by confocal microscopy (Zeiss LSM 510, Carl Zeiss AG, Oberkochen, Germany).

Conflict of Interest: M. V. McConnell receives research support from GE Healthcare and is on a scientific advisory board for Kowa, Inc. M. Terashima has received honoraria from Philips Electronics Japan. The other authors have no potential conflicts of interest.

Acknowledgment. This work was supported by a grant from the National Institute of Health, R01-HL078678 (M.V.M.) and the National Institute of Biomedical Imaging and Bioengineering, R21EB005364 (T.D.).

Supporting Information Available: Amino acid sequence of the HspG41C and LyP-Hsp, MS of the IAA-labeled protein cages, and scheme of experimental protocol for establishment of macrophage-rich murine carotid lesions are available. This material is available free of charge *via* the Internet at http://pubs.acs.org.

REFERENCES AND NOTES

1. Farokhzad, O. C.; Langer, R. Nanomedicine: Developing Smarter Therapeutic and Diagnostic Modalities. *Adv. Drug Delivery Rev.* **2006,** *58*, 1456–1459.
2. Emerich, D. F.; Thanos, C. G. The Pinpoint Promise of Nanoparticle-Based Drug Delivery and Molecular Diagnosis. *Biomol. Eng.* **2006,** *23*, 171–184.
3. Malam, Y.; Loizidou, M.; Seifalian, A. M. Liposomes and Nanoparticles: Nanosized Vehicles for Drug Delivery in Cancer. *Trends Pharmacol. Sci.* **2009,** *30*, 592–599.
4. Torchilin, V. P. Micellar Nanocarriers: Pharmaceutical Perspectives. *Pharm. Res.* **2007,** *24*, 1–16.
5. Douglas, T.; Young, M. Viruses: Making Friends with Old Foes. *Science* **2006,** *312*, 873–875.
6. Uchida, M.; Klem, M.; Allen, M.; Suci, P.; Flenniken, M.; Gillitzer, E.; Varpness, Z.; Liepold, L.; Young, M.; Douglas, T. Biological Containers: Protein Cages as Multifunctional Nanoplatforms. *Adv. Mater.* **2007,** *19*, 1025–1042.
7. Flenniken, M. L.; Willits, D. A.; Harmsen, A. L.; Liepold, L. O.; Harmsen, A. G.; Young, M. J.; Douglas, T. Melanoma and Lymphocyte Cell-Specific Targeting Incorporated into a Heat Shock Protein Cage Architecture. *Chem. Biol.* **2006,** *13*, 161–170.
8. Kovacs, E. W.; Hooker, J. M.; Romanini, D. W.; Holder, P. G.; Berry, K. E.; Francis, M. B. Dual-Surface-Modified Bacteriophage MS2 as an Ideal Scaffold for a Viral Capsid-Based Drug Delivery System. *Bioconjugate Chem.* **2007,** *18*, 1140–1147.
9. Datta, A.; Hooker, J.; Botta, M.; Francis, M.; Aime, S.; Raymond, K. High Relaxivity Gadolinium Hydroxypyridonate-Viral Capsid Conjugates: Nanosized MRI Contrast Agents1. *J. Am. Chem. Soc.* **2008,** *130*, 2546–2552.
10. Uchida, M.; Flenniken, M. L.; Allen, M.; Willits, D. A.; Crowley, B. E.; Brumfield, S.; Willis, A. F.; Jackiw, L.; Jutila, M.; Young, M. J.; *et al.* Targeting of Cancer Cells with Ferrimagnetic Ferritin Cage Nanoparticles. *J. Am. Chem. Soc.* **2006,** *128*, 16626–16633.
11. Liepold, L. O.; Abedin, M. J.; Buckhouse, E. D.; Frank, J. A.; Young, M. J.; Douglas, T. Supramolecular Protein Cage Composite MR Contrast Agents with Extremely Efficient Relaxivity Properties. *Nano Lett.* **2009,** *9*, 4520–4526.
12. Hooker, J. M.; Datta, A.; Botta, M.; Raymond, K. N.; Francis, M. B. Magnetic Resonance Contrast Agents from Viral Capsid Shells: A Comparison of Exterior and Interior Cargo Strategies. *Nano Lett.* **2007,** *7*, 2207–2210.
13. Lewis, J. D.; Destito, G.; Zijlstra, A.; Gonzalez, M. J.; Quigley, J. P.; Manchester, M.; Stuhlmann, H. Viral Nanoparticles as Tools for Intravital Vascular Imaging. *Nat. Med.* **2006,** *12*, 354–360.

14. Anderson, E. A.; Isaacman, S.; Peabody, D. S.; Wang, E. Y.; Canary, J. W.; Kirshenbaum, K. Viral Nanoparticles Donning a Paramagnetic Coat: Conjugation of MRI Contrast Agents to the MS2 Capsid. *Nano Lett.* **2006,** *6*, 1160–1164.
15. Destito, G.; Yeh, R.; Rae, C. S.; Finn, M. G.; Manchester, M. Folic Acid-Mediated Targeting of Cowpea Mosaic Virus Particles to Tumor Cells. *Chem. Biol.* **2007,** *14*, 1152–1162.
16. Soto, C. M.; Blum, A. S.; Vora, G. J.; Lebedev, N.; Meador, C. E.; Won, A. P.; Chatterji, A.; Johnson, J. E.; Ratna, B. R. Fluorescent Signal Amplification of Carbocyanine Dyes Using Engineered Viral Nanoparticles. *J. Am. Chem. Soc.* **2006,** *128*, 5184–5189.
17. Hooker, J.; O'neil, J.; Romanini, D.; Taylor, S.; Francis, M. B. Genome-Free Viral Capsids as Carriers for Positron Emission Tomography Radiolabels. *Mol. Imaging Biol.* **2008,** *10*, 182–191.
18. Kim, K. K.; Kim, R.; Kim, S. H. Crystal Structure of a Small Heat-Shock Protein. *Nature* **1998,** *394*, 595–599.
19. World Health Organization. The top 10 cause of death; available from http://www.who.int/mediacentre/factsheets/fs310/en/index.html.
20. Libby, P.; Aikawa, M. Stabilization of Atherosclerotic Plaques: New Mechanisms and Clinical Targets. *Nat. Med.* **2002,** *8*, 1257–1262.
21. Libby, P. Inflammation in Atherosclerosis. *Nature* **2002,** *420*, 868–874.
22. Ross, R. Mechanisms of Disease—Atherosclerosis: An Inflammatory Disease. *N. Engl. J. Med.* **1999,** *340*, 115–126.
23. Jaffer, F. A.; Libby, P.; Weissleder, R. Molecular and Cellular Imaging of Atherosclerosis—Emerging Applications. *J. Am. Coll. Cardiol.* **2006,** *47*, 1328–1338.
24. Laakkonen, P.; Porkka, K.; Hoffman, J. A.; Ruoslahti, E. A Tumor-Homing Peptide with a Targeting Specificity Related to Lymphatic Vessels. *Nat. Med.* **2002,** *8*, 751–755.
25. Fogal, V.; Zhang, L.; Krajewski, S.; Ruoslahti, E. Mitochondrial/Cell-Surface Protein p32/gC1qR as a Molecular Target in Tumor Cells and Tumor Stroma. *Cancer Res.* **2008,** *68*, 7210–7218.
26. Flenniken, M. L.; Willits, D. A.; Brumfield, S.; Young, M.; Douglas, T. The Small Heat Shock Protein Cage from *Methanococcus Jannaschii* Is a Versatile Nanoscale Platform for Genetic and Chemical Modification. *Nano Lett.* **2003,** *3*, 1573–1576.
27. Cuschieri, J. Implications of Lipid Raft Disintegration: Enhanced Anti-Inflammatory Macrophage Phenotype. *Surgery* **2004,** *136*, 169–175.
28. Ide, N.; Keller, C.; Weiss, N. Aged Garlic Extract Inhibits Homocysteine-Induced CD36 Expression and Foam Cell Formation in Human Macrophages. *J. Nutr.* **2006,** *136*, 755S–758S.
29. Terashima, M.; Uchida, M.; Kosuge, H.; Tsao, P. S.; Young, J. M.; Conolly, S. M.; Douglas, T.; McConnell, M. V. Human Ferritin for Macrophage Imaging in Atherosclerosis. *Biomaterial* **2011,** *32*, 1430–1437.
30. Jaffer, F. A.; Libby, P.; Weissleder, R. Molecular Imaging of Cardiovascular Disease. *Circulation* **2007,** *116*, 1052–1061.
31. Davies, J. R.; Rudd, J. H. F.; Weissberg, P. L.; Narula, J. Radionuclide Imaging for the Detection of Inflammation in Vulnerable Plaques. *J. Am. Coll. Cardiol.* **2006,** *47*, C57–C68.
32. Amirbekian, V.; Lipinski, M. J.; Briley-Saebo, K. C.; Amirbekian, S.; Aguinaldo, J. G. S.; Weinreb, D. B.; Vucic, E.; Frias, J. C.; Hyafil, F.; Mani, V.; *et al.* Detecting and Assessing Macrophages *In Vivo* To Evaluate Atherosclerosis Noninvasively Using Molecular MRI. *Proc. Natl. Acad. Sci. U.S.A.* **2007,** *104*, 961–966.
33. Ohtsuki, K.; Hayase, M.; Akashi, K.; Kopiwoda, S.; Strauss, H. W. Detection of Monocyte Chemoattractant Protein-1 Receptor Expression in Experimental Atherosclerotic Lesions—An Autoradiographic Study. *Circulation* **2001,** *104*, 203–208.
34. Deguchi, J.; Aikawa, M.; Tung, C. H.; Aikawa, E.; Kim, D. E.; Ntziachristos, V.; Weissleder, R.; Libby, P. Inflammation in Atherosclerosis—Visualizing Matrix Metalloproteinase Action in Macrophages *In Vivo*. *Circulation* **2006,** *114*, 55–62.
35. Arap, W.; Pasqualini, R.; Ruoslahti, E. Cancer Treatment by Targeted Drug Delivery to Tumor Vasculature in a Mouse Model. *Science* **1998,** *279*, 377–380.
36. Uchida, M.; Willits, A. D.; Muller, K.; Willis, A. F.; Jackiw, L.; Jutila, M.; Young, M.; Porter, A. E.; Douglas, T. Intracellular Distribution of Macrophage Targeting Ferriti-Iron Oxide Nanocomposite. *Adv. Mater.* **2009,** *21*, 458–462.
37. Montet, X.; Funovics, M.; Montet-Abou, K.; Weissleder, R.; Josephson, L. Multivalent Effects of RGD Peptides Obtained by Nanoparticle Display. *J. Med. Chem.* **2006,** *49*, 6087–6093.
38. Graves, E. E.; Yessayan, D.; Turner, G.; Weissleder, R.; Ntziachristos, V. Validation of *In Vivo* Fluorochrome Concentrations Measured Using Fluorescence Molecular Tomography. *J. Biomed. Opt.* **2005,** 10.
39. Kooi, M. E.; Cappendijk, V. C.; Cleutjens, K.; Kessels, A. G. H.; Kitslaar, P.; Borgers, M.; Frederik, P. M.; Daemen, M.; van Engelshoven, J. M. A. Accumulation of Ultrasmall Superparamagnetic Particles of Iron Oxide in Human Atherosclerotic Plaques Can Be Detected by *In Vivo* Magnetic Resonance Imaging. *Circulation* **2003,** *107*, 2453–2458.
40. Trivedi, R. A.; U-King-Im, J. M.; Graves, M. J.; Cross, J. J.; Horsley, J.; Goddard, M. J.; Skepper, J. N.; Quartey, G.; Warburton, E.; Joubert, I.; *et al. In Vivo* Detection of Macrophages in Human Carotid Atheroma—Temporal Dependence of Ultrasmall Superparamagnetic Particles of Iron Oxide-Enhanced MRI. *Stroke* **2004,** *35*, 1631–1635.
41. Yancy, A. D.; Olzinski, A. R.; Hu, T. C. C.; Lenhard, S. C.; Aravindhan, K.; Gruver, S. M.; Jacobs, P. M.; Willette, R. N.; Jucker, B. M. Differential Uptake of Ferumoxtran-10 and Ferumoxytol, Ultrasmall Superparamagnetic Iron Oxide Contrast Agents in Rabbit: Critical Determinants of Atherosclerotic Plaque Labeling. *J. Magn. Reson. Imaging* **2005,** *21*, 432–442.
42. Maiseyeu, A.; Mihai, G.; Kampfrath, T.; Simonetti, O. P.; Sen, C. K.; Roy, S.; Rajagopalan, S.; Parthasarathy, S. Gadolinium Containing Phosphatidylserine Liposomes for Molecular Imaging of Atherosclerosis. *J. Lipid Res.* **2008,** *50*, 2157–2163.
43. Kosuge, H.; Sherlock, S. P.; Kitagawa, T.; Terashima, M.; Barral, J. K.; Nishimura, D. G.; Dai, H.; Mcconnell, M. V. FeCo/Graphite Nanocrystals for Multi-Modality Imaging of Experimental Vascular Inflammation. *PLoS ONE* **2011,** *6*, e14523.
44. Hyafil, F.; Cornily, J. C.; Feig, J. E.; Gordon, R.; Vucic, E.; Amirbekian, V.; Fisher, E. A.; Fuster, V.; Feldman, L. J.; Fayad, Z. A. Noninvasive Detection of Macrophages Using a Nanoparticulate Contrast Agent for Computed Tomography. *Nat. Med.* **2007,** *13*, 636–641.
45. Nahrendorf, M.; Zhang, H. W.; Hembrador, S.; Panizzi, P.; Sosnovik, D. E.; Aikawa, E.; Libby, P.; Swirski, F. K.; Weissleder, R. Nanoparticle PET-CT Imaging of Macrophages in Inflammatory Atherosclerosis. *Circulation* **2008,** *117*, 379–387.
46. Nahrendorf, M.; Sosnovik, D. E.; Weissleder, R. MR-Optical Imaging of Cardiovascular Molecular Targets. *Basic Res. Cardiol.* **2008,** *103*, 87–94.
47. Rudd, J. H. F.; Warburton, E. A.; Fryer, T. D.; Jones, H. A.; Clark, J. C.; Antoun, N.; Johnstrom, P.; Davenport, A. P.; Kirkpatrick, P. J.; Arch, B. N.; *et al.* Imaging Atherosclerotic Plaque Inflammation with [F-18]-Fluorodeoxyglucose Positron Emission Tomography. *Circulation* **2002,** *105*, 2708–2711.
48. Ogawa, M.; Ishino, S.; Mukai, T.; Asano, D.; Teramoto, N.; Watabe, H.; Kudomi, N.; Shiomi, M.; Magata, Y.; Iida, H.; *et al.* F-18-FDG Accumulation in Atherosclerotic Plaques: Immunohistochemical and PET Imaging Study. *J. Nucl. Med.* **2004,** *45*, 1245–1250.
49. Allen, M.; Bulte, J. W. M.; Liepold, L.; Basu, G.; Zywicke, H. A.; Frank, J. A.; Young, M.; Douglas, T. Paramagnetic Viral Nanoparticles as Potential High-Relaxivity Magnetic Resonance Contrast Agents. *Magn. Reson. Med.* **2005,** *54*, 807–812.
50. Liepold, L.; Anderson, S.; Willits, D.; Oltrogge, L.; Frank, J. A.; Douglas, T.; Young, M. Viral Capcids as MRI Contrast Agents. *Magn. Reson. Med.* **2007,** *58*, 871–879.

51. Uchida, M.; Terashima, M.; Cunningham, C. H.; Suzuki, Y.; Willits, D. A.; Willis, A. F.; Yang, P. C.; Tsao, P. S.; McConnell, M. V.; Young, M. J.; *et al.* A Human Ferritin Iron Oxide Nano-Composite Magnetic Resonance Contrast Agent. *Magn. Reson. Med.* **2008,** *60*, 1073–1081.
52. Hooker, J. M.; O'Neil, J. P.; Romanini, D. W.; Taylor, S. E.; Francis, M. B. Genome-Free Viral Capsids as Carriers for Positron Emission Tomography Radiolabels. *Mol. Imaging Biol.* **2008,** *10*, 182–191.
53. Prasuhn, D. E.; Yeh, R. M.; Obenaus, A.; Manchester, M.; Finn, M. G. Viral MRI Contrast Agents: Coordination of Gd by Native Virions and Attachment of Gd Complexes by Azide-Alkyne Cycloaddition. *Chem. Commun.* **2007,** 1269–1271.
54. Chatterji, A.; Burns, L. L.; Taylor, S. S.; Lomonossoff, G. P.; Johnson, J. E.; Lin, T.; Porta, C. Cowpea Mosaic Virus: From the Presentation of Antigenic Peptides to the Display of Active Biomaterials. *Intervirology* **2002,** *45*, 362–370.
55. Suci, P. A.; Varpness, Z.; Gillitzer, E.; Douglas, T.; Young, M. Targeting and Photodynamic Killing of a Microbial Pathogen Using Protein Cage Architectures Functionalized with a Photosensitizer. *Langmuir* **2007,** *23*, 12280–12286.
56. Rae, C. S.; Khor, I. W.; Wang, Q.; Destito, G.; Gonzalez, M. J.; Singh, P.; Thomas, D. M.; Estrada, M. N.; Powell, E.; Finn, M. G.; *et al.* Systemic Trafficking of Plant Virus Nanoparticles in Mice *via* the Oral Route. *Virology* **2005,** *343*, 224–235.
57. Singh, P.; Prasuhn, D.; Yeh, R. M.; Destito, G.; Rae, C. S.; Osborn, K.; Finn, M. G.; Manchester, M. Bio-Distribution, Toxicity and Pathology of Cowpea Mosaic Virus Nanoparticles *In Vivo*. *J. Controlled Release* **2007,** *120*, 41–50.
58. Kaiser, C. R.; Flenniken, M. L.; Gillitzer, E.; Harmsen, A. L.; Harmsen, A. G.; Jutila, M. A.; Douglas, T.; Young, M. J. Biodistribution Studies of Protein Cage Nanoparticles Demonstrate Broad Tissue Distribution and Rapid Clearance *In Vivo*. *Int. J. Nanomed.* **2007,** *2*, 715–733.
59. Shevchenko, A.; Tomas, H.; Havli\[Sbreve, J.; Olsen, J. V.; Mann, M. In-Gel Digestion for Mass Spectrometric Characterization of Proteins and Proteomes. *Nat. Protoc.* **2006,** *1*, 2856–2860.
60. Tsuchiya, S.; Kobayashi, Y.; Goto, Y.; Okumura, H.; Nakae, S.; Konno, T.; Tada, K. Induction of Maturation in Cultured Human Monocytic Leukemia-Cells by a Phorbol Diester. *Cancer Res.* **1982,** *42*, 1530–1536.
61. Benedetto, S.; Pulito, R.; Crich, S. G.; Tarone, G.; Aime, S.; Silengo, L.; Hamm, J. Quantification of the Expression Level of Integrin Receptor $\alpha_v\beta_3$ in Cell Lines and MR Imaging with Antibody-Coated Iron Oxide Particles. *Magn. Reson. Med.* **2006,** *56*, 711–716.
62. Lichtman, A. H.; Clinton, S. K.; Iiyama, K.; Connelly, P. W.; Libby, P.; Cybulsky, M. I. Hyperlipidemia and Atherosclerotic Lesion Development in LDL Receptor-Deficient Mice Fed Defined Semipurified Diets with and without Cholate. *Arterioscler. Thromb. Vasc. Biol.* **1999,** *19*, 1938–1944.